Published in final edited form as:
J Biol Chem. 2008 January 18; 283(3): 1401–1410. doi:10.1074/jbc.M703831200.

Acidic/IQ Motif Regulator of Calmodulin*

John A. Putkey[‡,1], **M. Neal Waxham**[§], **Tara R. Gaertner**[§], **Kari J. Brewer**[‡], **Michael Goldsmith**[‡], **Yoshihisa Kubota**[§], and **Quinn K. Kleerekoper**[‡]

[‡]Department of Biochemistry and Molecular Biology, University of Texas, Houston Medical School, Houston, Texas 77030

[§]Department of Neurobiology and Anatomy, University of Texas, Houston Medical School, Houston, Texas 77030

Abstract

The small IQ motif proteins PEP-19 (62 amino acids) and RC3 (78 amino acids) greatly accelerate the rates of Ca^{2+} binding to sites III and IV in the C-domain of calmodulin (CaM). We show here that PEP-19 decreases the degree of cooperativity of Ca^{2+} binding to sites III and IV, and we present a model showing that this could increase Ca^{2+} binding rate constants. Comparative sequence analysis showed that residues 28 to 58 from PEP-19 are conserved in other proteins. This region includes the IQ motif (amino acids 39–62), and an adjacent acidic cluster of amino acids (amino acids 28–40). A synthetic peptide spanning residues 28–62 faithfully mimics intact PEP-19 with respect to increasing the rates of Ca^{2+} association and dissociation, as well as binding preferentially to the C-domain of CaM. In contrast, a peptide encoding only the core IQ motif does not modulate Ca^{2+} binding, and binds to multiple sites on CaM. A peptide that includes only the acidic region does not bind to CaM. These results show that PEP-19 has a novel acidic/IQ CaM regulatory motif in which the IQ sequence provides a targeting function that allows binding of PEP-19 to CaM, whereas the acidic residues modify the nature of this interaction, and are essential for modulating Ca^{2+} binding to the C-domain of CaM.

Calmodulin (CaM)[2] is a 17-kDa Ca^{2+} receptor found in all eukaryotic cells, where it regulates activities ranging from neural transmission to growth and differentiation (for a condensed review see Ref. 1). This daunting task requires that CaM interact with a large number of proteins and that it properly sense Ca^{2+} signals that vary greatly in frequency and amplitude (for review see Refs. 2 and 3). To effectively fulfill its diverse roles, mechanisms have evolved to regulate, or fine-tune CaM activity over short time frames. For example, phosphorylation of a small protein called ARPP-21 promotes high affinity binding to Ca^{2+}-CaM, (neurogranin or Ng) thereby competitively inhibiting activation of other CaM-dependent enzymes (4).

PEP-19 (Purkinje cell protein 4 or pcp4) and RC3 (neurogranin or Ng) are small proteins expressed primarily in neuronal tissues, but with no known activity other than binding to

*This work was supported in part by National Institutes of Health Grants GM069611 and NS038310 and Robert A. Welch Foundation Grant AU1144.

[1]To whom correspondence should be addressed: 6431 Fannin St., Houston, TX 77030. Fax: 713-500-0651; john.putkey@uth.tmc.edu.

[2]The abbreviations used are: CaM, calmodulin; Ca^{2+}-CaM, Ca^{2+}-bound calmodulin; CaM_{ACR}, acrylodan labeled CaM(K75C); CaM_{DANS}, IAEDANS labeled CaM(K75C); CKII, CaM-dependent protein kinase II; RC3, neurogranin; FRET, fluorescence resonance energy transfer; MOPS, 4-morpholinepropane-sulfonic acid; acrylodan, 6-acryloyl-2-dimethylaminonaphthalene; IAEDANS, 5-((((2-iodoacetyl)amino)ethyl)amino)naphthalene-1-sulfonic acid; DDPM, *N*-(4-dimethylamino-3,5-dinitrophenyl)maleimide; HPLC, high performance liquid chromatography; Br_2, 5,5′-dibromo; BAPTA, 1,2-bis(2-aminophenoxy)ethane-*N*,*N*,*N*′,*N*′-tetraacetic acid.

CaM in the presence or absence of Ca^{2+}. We found that both PEP-19 and RC3 have profound effects on the rate-limiting kinetics of Ca^{2+} binding to the C-domain of CaM. Specifically, PEP-19 accelerates the rates of both association and dissociation of Ca^{2+} without greatly affecting the overall K_{Ca} of the C-domain (5). RC3 accelerates the rate of Ca^{2+} dissociation from CaM, but has a lesser effect on the association rate, thereby decreasing the affinity of binding Ca^{2+} to the C-domain of CaM (6). Importantly, both PEP-19 and RC3 exert these effects even when CaM is bound to CaM-dependent protein kinase II (CKIIα) (5, 6).

These results suggest that PEP-19 and RC3 could have broad extrinsic effects on CaM-related signaling pathways by modulating the Ca^{2+} binding properties of free or enzyme-bound CaM. This is consistent with the phenotype of RC3 knock-out mice, which show defects in synaptic plasticity (7), attenuated phosphorylation of hippocampal protein kinase A and C substrates (8), and altered Ca^{2+} dynamics in cortical neurons (9).

Both PEP-19 and RC3 contain an IQ motif. This rather loose consensus sequence (IQ*XXX*RG*XXX*R) was first identified as the light chain binding site in conventional myosins, but was subsequently recognized as a CaM binding sequence in numerous other proteins (10). IQ motif proteins exhibit diverse modes of interaction with CaM that include Ca^{2+}-dependent or independent binding (10), binding to both or only one domain of CaM (5, 11–13), binding multiple CaMs to multiple IQ motifs (14), and exchange of CaM between the IQ motif and other sites in the same protein (15, 16).

These intriguing structure-function relationships of IQ motifs led us to identify amino acids in PEP-19 that are required to modulate Ca^{2+} binding to CaM. We show here that the consensus IQ CaM binding motif is necessary, but not sufficient to mimic the effect of intact PEP-19 on CaM. An adjacent highly acidic amino acid sequence acts in synergy with the IQ motif to modulate Ca^{2+} binding to the C-domain of CaM. We propose that this acidic/IQ sequence constitutes a new CaM regulatory motif.

EXPERIMENTAL PROCEDURES

Recombinant Proteins and Peptides

Recombinant CaM, CaM(K75C), CaM(T110C), CaM(T34C), CaM(T34C, T110C), PEP19, and RC3 were cloned, expressed, and purified as described previously (5, 6, 16–18). The expression plasmid for the C-domain of CaM (residues 78–148) was a generous gift from Dr. Madeline Shea (University of Iowa). Synthetic peptides purchased from Sigma Genosys had greater than 90% purity, and were further purified as necessary by C4 reverse phase HPLC using 0–60% acetonitrile gradient in water, 0.1% trifluoroacetic acid.

NMR Methodology

NMR spectra of isotope-labeled CaM and PEP-19 were generated using Varian Inova 800 MHz and Bruker DRX800 MHz spectrometers with room temperature triple resonance probes, as well as a Bruker DRX 600 MHz spectrometer equipped with 5-mm TXI CryoProbe. Backbone assignments for Ca^{2+}-CaM in the absence and presence of PEP-19 were reported previously (5). Titration of $[^{15}N]Ca^{2+}$-CaM with PEP-19 or peptides was performed in a buffer containing 10 mM imidazole, pH 6.3, 100 mM KCl, 5 mM $CaCl_2$, 5% D_2O at 310 or 320 K. Amide chemical shifts in the ^{15}N,^{1}H-heteronuclear single quantrum coherence spectra for $[^{15}N]Ca^{2+}$-CaM exhibited fast exchange characteristics during titration with PEP-19, PEP(28–62), or PEP(39–62), which allowed assignments to be made by following chemical shift changes from the free to bound forms of CaM. All titrations were conducted at a CaM concentration of 50 μM. To eliminate dilution and pH effects, titrations were made from a stock solution of concentrated unlabeled PEP-19 or peptides

containing 50 μM Ca^{2+}-CaM in the appropriate buffer. At each titration point a measured amount of sample was removed from the NMR tube and replaced with the identical volume from the stock solution. Titrations were carried out until a 10-fold excess of ligand was added. The data were processed using the Auto-screen module in FELIX 2002 software (19). The average amide chemical shift change was calculated using the following formula:

$$\Delta\delta \text{ avg} = \sqrt{\frac{(\Delta\delta H)^2 + (\Delta\delta N/5)^2}{2}} \quad \text{(Eq. 1)}$$

where $\Delta\delta H$ = change in ^{1}H chemical shift and $\Delta\delta n$ = change in ^{15}N chemical shift.

Chemical shift changes for CaM backbone amide ^{1}H and ^{15}N nuclei were analyzed separately to derive K_d values for binding PEP-19 to CaM because the relative contribution of change in each dimension can vary significantly. In general, backbone ^{15}N chemical shifts experienced the greatest change relative to the spectral window.

Generation of Fluorescently Labeled Proteins

Labeling of CaM(K75C) or CaM(T110C) with either acylodan or IAEDANS was previously reported (18, 20). To obtain the fluorescent CaM used in the FRET study, a double Cys CaM mutant, CaM(T34C, T110C), was labeled with IAEDANS (donor) and DDPM (accepter) to generate CaMD/A. CaM(T34C, T110C) was first reacted with 0.4 mol of IAEDANS/mol of protein in 20 mM Tris-HCl at pH 7.5 and 100 mM KCl for 2 h at 20 °C in the dark. Free IAEDANS was removed using a Bio-Gel P-6DG (Bio-Rad) desalting column. The IAEDANS-labeled CaM averaged 0.3 mol of IAEDANS/mol of protein. A portion of this partially labeled protein was saved as the donor-alone protein (CaMD), whereas the rest was labeled with excess DDPM to give CaMD/A. Free DDPM was removed by desalting. PEP-19 and PEP (39–62) with C-terminal Gly-Cys extensions were labeled with DDPM as described for CaM, but free DDPM was removed using a semi-prep C4 reverse phase HPLC column with a 0–60% acetonitrile gradient. Protein and peptide concentrations were determined using the Pierce BCA protein assay with a bovine serum albumin standard and color developed at 60 °C.

Equilibrium Binding of PEP-19 to CaM

Solutions of fluorescently labeled CaM derivatives were prepared in a buffer of 20 mM MOPS, pH 7.5, 100 mM KCl, and 1 mM dithiothreitol. Concentrated stock solutions of PEP-19, PEP(39–62), or their DDPM-labeled derivatives, were prepared by dissolving lyophilized protein or peptide in the labeled CaM solution to eliminate dilution of CaM during titration. The increase in volume was less than 10%. We assessed potential nonspecific FRET effects using DDPM coupled to free Cys, and found a linear, 5% decrease in fluorescence from donor-labeled CaM per increment of 25 μM Cys-DDPM. The FRET effect between donor-labeled CaM and acceptor-labeled PEP-19 or PEP(39–62) was corrected for this nonspecific effect, and the upper concentration of DDPM-labeled ligands was limited to 50 μM.

Dissociation constants (K_d) were derived from fluorescence or NMR data by fitting titration curves to the following equation, which does not require measurement of free ligand concentrations,

$$S = S_i + (S_f - S_i)\left(\frac{(L + C_t + K_d) - \sqrt{(L + C_t + K_d)^2 - 4C_tL}}{2C_t}\right) \quad \text{(Eq. 2)}$$

Where S = fluorescence or NMR signal at a given titration point; S_i = initial signal in the absence of ligand; S_f = final signal in the presence of excess ligand; L = total ligand added at a given titration point; C_t = total CaM concentration; and K_d = dissociation constant. The equation was used to fit plots of S *versus* L with S_i, S_f, and K_d as fitted variables.

Equilibrium Ca^{2+} Binding

Macroscopic equilibrium Ca^{2+} binding constants were determined using the competitive binding assay described by Linse *et al.* (21). Calcium was removed from buffers by passage over a Calcium-Sponge column (Molecular Probes). Residual Ca^{2+} detected using Indo-1 was typically $<10^{-7}$ M. CaM was decalcified by adding 1–5 mM BAPTA followed by desalting into Ca^{2+}-free buffers. This effectively removed greater than 95% of Ca^{2+} from CaM as determined by Tyr fluorescence. All pipette tips, cuvettes, and other labware were rinsed with 0.1 M HCl and MilliQ water to remove Ca^{2+}.

Samples used for equilibrium binding studies contained 30 μM CaM, 30 μM 5,5′-dibromo-BAPTA (Br_2BAPTA; Molecular Probes/Invitrogen; K_d = 1.59 μM), with or without 60 μM PEP-19 polypeptides, in a buffer of 20 mM MOPS, pH 7.5, 100 mM KCl. Calcium was added from a stock solution prepared in a buffer that contained both CaM and Br_2BAPTA such that only the Ca^{2+} concentration varied during the titration. Titrations were performed by addition of 2-, 3-, 5-, or 10-μl aliquots of the Ca^{2+} stock, to an initial sample volume of 0.7 ml. The decrease in absorbance of Br_2BAPTA at 263 nm was monitored using a Cary/Varian 100 spectrophotometer. The number and volume of aliquots was adjusted to achieve an even distribution of data points on the binding isotherm. The total Ca^{2+} concentration was then calculated based on the initial volume and total added volume at each titration point. Macroscopic calcium binding constants were calculated essentially as described by Linse *et al.* (21) using the following equations,

$$[\mathrm{Ca}]_F = \frac{K_{d(\mathrm{BAP})} \times (\mathrm{Abs}_{\mathrm{MAX}} - \mathrm{Abs})}{(\mathrm{Abs} - \mathrm{Abs}_{\mathrm{MIN}})} \quad \text{(Eq. 3)}$$

$$[\mathrm{Ca}]_T = [\mathrm{Ca}]_F + \frac{[\mathrm{Ca}]_F \times [\mathrm{BAP}]}{[\mathrm{Ca}]_F + K_{d(\mathrm{BAP})}} + \frac{\mathrm{F} \times [\mathrm{pro}] \times \sum_{k=1}^{N} \left(k \times [\mathrm{Ca}]_F{}^k \times \prod_{j=1}^{k} K_j \right)}{1 + \sum_{k=1}^{N} \left([\mathrm{Ca}]_F{}^k \times \prod_{j=1}^{k} K_j \right)} \quad \text{(Eq. 4)}$$

Where $[Ca]_T$ = total Ca^{2+}; $[Ca]_F$ = concentration of free Ca^{2+}; [Pro] = concentration of CaM; [BAP] = concentration of Br_2BAPTA; $K_{d(BAP)}$ = Ca^{2+} dissociation constant for Br_2BAPTA; K = macromolecular binding constants for N number of sites (K_1 through K_4); and Abs_{MAX}, Abs_{MIN}, and Abs are the absorbance of Br_2BAPTA in the absence, at saturating, and at intermediate concentrations of Ca^{2+}, respectively. Because the stoichiometry of Ca^{2+} binding is very sensitive to small errors in protein concentration, we incorporated factor F to compensate for slight errors in CaM protein concentrations as done by Linse *et al.* (21). Plots of $[Ca]_T$ *versus* Abs were fit directly to Equation 4 by least squares using Kaleidagraph software. The fitted variables were the macroscopic binding constants, F, Abs_{MAX}, and Abs_{MIN}. Values for F were typically greater than 0.8. The Ca^{2+} binding constant for Br_2BAPTA of 1.59×10^{-6} was experimentally determined at the same pH and ionic strength used in the binding assay.

Stopped-flow Measurements

Stopped-flow fluorescence experiments were performed at 23 °C using an Applied Photophysics Ltd. (Leatherhead, UK) Model SX.18 MV sequential stopped-flow spectrofluorimeter with a 150 watt Xe/Hg lamp, and a dead time of 1.7 ms. All solutions contained a base buffer of 20 mM MOPS, pH 7.5, 100 mM KCl. The concentration of other reagents in stopped-flow mixing solutions A and B are defined in the figure legends. The final concentration of these reagents in the optical chamber was one-half of these values, because the mixing ratio was 1:1.

Calcium k_{off} rates were determined using 2 μM CaM, 20 μM Ca^{2+}, and 300 μM Quin-2. Fluorescence from Quin-2 was detected using an excitation wavelength of 334.5 nm and Oriel emission cut-off filter 51282. A stopped-flow experiment to measure Ca^{2+} k_{on} rates was devised using the Ca^{2+}-sensitive chromophore Br_2BAPTA as a buffer to maintain free Ca^{2+}levels in the range of 0.5 to 5μM, and as a chromophore to monitor Ca^{2+}binding. The kinetics of binding $Ca^{2+}$to Br_2BAPTA and the N-domain of CaM are very fast and thus, the increase in absorbance observed upon mixing apo-CaM with Ca^{2+}/Br_2BAPTA solutions is due to the release of $Ca^{2+}$from Ca^{2+}/Br_2BAPTA as Ca^{2+}binds to the C-domain of CaM. The observed change in absorbance was fitted to a single exponential equation. All buffers contained 20 mM MOPS, pH 7.5, and 100 mM KCl. The assay was performed at 20 °C. Typically, Buffer A contained 5 μM BAPTA with or without 2 to 4 μM decalcified CaM or EGTA, whereas Buffer B contained 250 μM Br_2BAPTA and sufficient Ca^{2+} to achieve a desired free Ca^{2+} upon mixing equal volumes of Buffers A and B. This allows less than a 3% change in the concentrations of Br_2BAPTA and Ca^{2+}-Br_2BAPTA as Ca^{2+} binds to CaM, thereby maintaining a reasonably constant level of free Ca^{2+}.

Free Ca^{2+} levels of Ca^{2+} /Br_2BAPTA solutions were calculated from the absorbance at 263 nm (Abs_{obs}) *versus* controls in the absence (Abs_{min}) or presence (Abs_{max}) of excess Ca^{2+} using the following equation.

$$Ca^{2+}{}_{Free} = 1.59\mu M \times \frac{(Abs_{obs} - Abs_{min})}{(Abs_{max} - Abs_{obs})} \quad \text{(Eq. 5)}$$

Free Ca^{2+} levels in the optical chamber of the stopped-flow instrument at 20 °C and pH 7.5 were determined from the observed rates of binding Ca^{2+} to EGTA present in solution A (K_d = 0.038 μM, k_{off} = 0.53 s^{-1}, k_{on} = 13.8 μM^{-1} s^{-1}). Free Ca^{2+} levels were in close agreement when calculated based on Br_2BAPTA absorbance or observed rates of binding Ca^{2+} to EGTA.

Microscopic Kinetic Model for Ca^{2+} Binding to the C-domain of CaM

Linked differential equations for the forward and reverse microscopic binding events illustrated in Fig. 6*A* were incorporated into a computational model using Berkeley Madonna software. Initial parameter values were taken from the current study and literature reports. The overall average apparent dissociation constant (K_d or K_{Ca50}) of 2.3 ± 0.3 μM was derived from Table 2 and other reports using a variety of techniques at pH 7.4 to 7.5 with 90 to 100 mM KCl (5, 21–30). The macroscopic dissociation constants, K_{d1} and K_{d2}, correspond to sequential binding of the first and second Ca^{2+} ions, regardless of which site is filled first. Starting values for K_{d1} and K_{d2} given in Table 2 are very close to those reported with others (21, 22). The microscopic dissociation constants K_{dIII} and K_{dIV} correspond to binding the first Ca^{2+} to site III or IV, respectively, whereas $K_{dIII/IV}$ and $K_{dIV/III}$ correspond to binding the second Ca^{2+} when the other site is already occupied. The model includes algebraic relationships that relate macroscopic and microscopic association constants (K_a; $K_a = 1/K_d$) as follows, where c is the coupling factor (31).

$$K_1 = K_{III} + K_{IV} \qquad c = (K_1 \times K_2)/(\times K_{III} \times K_{IV})$$
$$K_{III/IV} = c \times K_{III} \quad K_{VI/III} = c \times K_{IV}$$

These relationships allow for the calculation of microscopic equilibrium binding constants if K_1, K_2, and the magnitude of difference between microscopic binding constants is known. K_1 and K_2 are reported in Table 2, and Evenas *et al.* (32) who used Ca^{2+} binding mutants to show that the relative Ca^{2+} binding affinity of site IV is ~6.3-fold greater than site III in both the 0-Ca^{2+} and 1-Ca^{2+} states of the C-domain.

Microscopic rate constants were constrained by the results of Malmendal *et al.* (32) who used NMR relaxation methods to conclude that the first Ca^{2+} ion binds preferentially to site IV, and that the k_{off} of site IV (k_{offIV}) was 5100 s^{-1}. If the 6.3-fold difference in affinity of binding Ca^{2+} to sites IV and III were due exclusively to k_{off} rates, then k_{offIII} would be = 32,000 s^{-1}, which is consistent with an exchange rate of 27,000 s^{-1} determined for transition between the open and closed conformation of the C-domain in which site IV was mutated (33). These k_{off} values would correspond to k_{onIV} and k_{onIII} rates of around 300 μM^{-1} s^{-1}, which is consistent with a diffusion-limited event, and similar to the k_{on} for Ca^{2+} binding to the N-domain of CaM. Microscopic rate constants for binding the second Ca^{2+} ion were constrained by the fact that the observed k_{off} ($k_{off,Obs}$) for dissociation of both Ca^{2+} ions from the C-domain measured using stopped-flow experiments described as above and best fits a single exponential rate between 8.5 s^{-1} and 12.6 s^{-1} (5, 25, 34, 35). Because NMR relaxation data show that the rate of dissociation of Ca^{2+} from the 1-Ca^{2+} state is very fast, then $k_{off,Obs}$ reflects the rate-limiting dissociation of the first Ca^{2+} from either site III or IV of the 2-Ca^{2+} state, followed by very rapid release of the second Ca^{2+}. This means that $k_{off,Obs} = k_{off,IV/III} + k_{off,III/IV}$, and it allows constraint of microscopic rate constants using the following relationships.

$$k_{off,III/IV} = k_{off,Obs} - k_{off,IV/III}$$
$$k_{on,III/IV} = (k_{off,Obs} - k_{off,IV/III})/k_{d,III/IV}$$
$$k_{on,IV/III} = k_{off,IV/III}/K_{d,IV/III}$$

Thus, k_{d}III/IV and k_{d}IV/III are calculated if $k_{off,Obs}$ is defined within an experimentally observed range, and $k_{off,IV/III}$ is varied between 0 and the defined $k_{off,Obs}$.

The model includes a Ca^{2+} buffer based on Br_2BAPTA with K_d = 1.59 μM, a diffusion limited k_{on} = 500 μM^{-1} s^{-1} and k_{off} = 795 s^{-1}. This allowed simulation of stopped-flow experiments described above to measure the rate of association of Ca^{2+} with the C-domain of CaM, and to use the built-in curve fit function of Berkeley Madonna to optimize parameter sets against experimental data.

Global parameter optimization and error analysis were also performed in the MATLAB computing environment (The MathWorks). Although the computational model (Fig. 1) has 8 kinetic parameter values, the experimental data and algebraic constraints described above and under “Results ” reduced the unknown parameters to $k_{on,III}$ and $k_{off,IV/III}$. However, to take into account the different reported values of $k_{off,Obs}$, we also treated $k_{off,III/IV}$ as an additional unknown parameter for the global optimization. We set the maximum values of $k_{on,III}$, $k_{off,IV/III}$, and $k_{off,III/IV}$ (500 μM^{-1} s^{-1}, 50 s^{-1}, and 50 s^{-1}, respectively) and divided the entire parameter space into 200 × 500 × 500 = 5 × 10^7 grid points. The error (root mean square difference) was calculated for each of these 5 × 10^7 grid points by comparing the simulated Ca^{2+} association and dissociation rates with the experimental data. This

systematic parameter optimization revealed a single distinct region of the parameter space in which the computational model best fit the data. The estimate of $k_{on,III}$ resulted in a unique set of parameter values of the model, which was again reconfirmed by the *lsqnonlin* function of the MATLAB Optimization Toolbox.

RESULTS

Identifying Sequences in PEP-19 That Bind to Ca^{2+}-CaM

A BLAST protein similarity search identified PEP-19 orthologs with high degrees of identity throughout their primary sequences. Other proteins of diverse size and from diverse species had sequence similarity to the C-terminal portion of PEP-19 that includes the IQ motif and cluster of adjacent acidic residues (see Fig. 1*A*). RC3 also has an acidic cluster but with a sequence that differs from PEP-19 (see "Discussion " for more details). The corresponding sequences from myosin V and the voltage-gated Ca^{2+} channel $Ca_v1.2$ are shown in Fig. 1*A* to emphasize the absence of acidic clusters in these IQ motif proteins.

The sequence comparisons in Fig. 1*A* led us to hypothesize that both the IQ motif and the adjacent acidic region in PEP-19 are necessary to modulate the Ca^{2+} binding of CaM. The peptides shown in Fig. 1*B* were synthesized to directly test this hypothesis. PEP(28–62) spans the acidic and IQ regions. PEP(39–62) includes the core IQ motif (10), and is the minimal region in PEP-19 shown to have CaM antagonist activity (36). PEP(28–45) encodes the acidic region without the IQ motif.

Intact PEP-19 and Its Consensus IQ Motif Peptide Have Divergent Effects on CaM Amide Chemical Shifts

The amide resonances of Ca^{2+}-CaM exhibit fast exchange characteristics on the NMR time scale upon titration with PEP-19, and are maximal at a CaM:PEP-19 ratio of 1:1. Fig. 2*A* shows that the greatest effects of PEP-19 are localized to the C-domain of Ca^{2+}-CaM, primarily in helix F, the linker between helices F and G, and in helix H. These data indicate a single major binding site for PEP-19 in the C-domain of Ca^{2+}-CaM.

Fig. 2, *A* and *B*, summarize the effects of PEP(28–62) and PEP(39–62) on the amide chemical shifts of Ca^{2+}-CaM. Both peptides caused chemical shift changes that were characteristic of fast exchange on the NMR time scale. It is clear that PEP(28–62) induces a pattern of chemical shift changes that is strikingly similar to that of intact PEP-19, with dominant effects on residues in the C-domain of CaM. In contrast, PEP(39–62) has pervasive effects on amide chemical shifts for residues in both the N- and C-domains of CaM, with clusters of perturbation localized to helical segments, especially helices C, D, F, and H.

PEP(28–45) showed only minor effects on the amide chemical shifts of Ca^{2+}-CaM, even when present at a molar excess of 100-fold (5 mM peptide *versus* 0.05 μM CaM). Thus, both the IQ motif and an adjacent group of acidic residues are necessary to mimic the effect of intact PEP-19 on CaM amide chemical shifts.

PEP-19 and Its Consensus IQ Motif Have Divergent Effects on the Global Conformation of CaM

CaM(T34C, T110C) with FRET donor and acceptor probes bound to N- and C-domains (CaMD/A) (16, 37) was used to determine the effect of PEP-19 derivatives on the global conformation of CaM. A peptide from CaM kinase II, CKII-(293–312) (20), was used as a positive control because it causes CaM to adopt a compact shape with the N- and C-domains in close proximity (38). Fig. 3 shows that binding CKII-(293–312) to Ca^{2+}-CaMD/A causes

a large decrease in fluorescence due to a FRET effect. PEP-19 and PEP(28–62) cause much smaller decreases in fluorescence, indicating they do not induce CaM to adopt a highly compact shape. CaM remains extended when bound to PEP(39–62) because fluorescence from CaMD/A is essentially unaffected by the peptide.

Relative Affinities of Binding PEP-19 Polypeptides to CaM

Fig. 4*A* plots Ca^{2+}-CaM amide chemical shifts as a function of increasing concentrations of PEP-19 or PEP(28–62). Both data sets fit well to a single-site binding model with K_d values of 29 and 24 μM for PEP-19 and PEP(28–62), respectively (see Table 1). Because PEP(39–62) affects amides in the N- and C-domains of Ca^{2+}-CaM, the average responses for selected residues in these domains were analyzed separately as shown in Fig. 4*B*. Chemical shift changes reached a maximum, but the chemical shift response curve for residues in the N-domain was right shifted relative to residues in the C-domain, suggesting that N-and C-domains sense different binding events. The *lines* in Fig. 4*B* show a fit to a single-site binding model, but the fits were poor relative to those shown in Fig. 4*A*. This was not surprising given the potential complexity of chemical shift changes in response to multiple ligands, and the high concentration of CaM required for NMR (50 μM) is not ideal for analysis of potentially high affinity binding events.

Fluorescence assays were also used to determine the relative affinities of binding PEP-19 and PEP(39–62) to CaM. Fig. 4*C* shows the effect of PEP-19 and PEP(39–62) on fluorescence intensity from acrylodan-labeled CaM(K75C), CaM_{ACR}. The data for intact PEP-19 fit a single-site model with a K_d of 18 μM (see Table 1). Interestingly, even though Figs. 2*C* and 3 indicate multiple binding sites for PEP(39–62) on Ca^{2+}-CaM, the response of Ca^{2+}-CaM_{ACR} to this peptide fit a single-site model with an apparent K_d of 0.24 μM. Thus, the affinity of binding PEP(39–62) to one site in Ca^{2+}-CaM is about 70-fold greater relative to binding intact PEP-19.

Fig. 4*D* shows results of a FRET assay using derivatives of PEP-19 and PEP(39–62) with C-terminal Cys residues labeled with the FRET acceptor DDPM, and CaM(T110C) labeled with the FRET donor IAEDANS. A large decrease in fluorescence of up to 70% due to FRET quenching was observed upon binding acceptor-labeled peptides to donor-labeled Ca^{2+}-CaM. Changes in fluorescence upon binding acceptor-labeled PEP-19 to donor-labeled Ca^{2+}-CaM fit a single-site model with a K_d of 20 μM, which is comparable with the values derived from both NMR and CaM_{ACR} (see Table 1). Interestingly, changes in fluorescence upon binding PEP(39–62) indicate at least two classes of binding sites. A K_d of 0.16 μM for the higher affinity site is comparable with that derived using CaM_{ACR}, whereas the K_d of 27 μM for the low affinity site is consistent with the K_d for binding intact PEP-19 to Ca^{2+}-CaM (see Table 1).

Together, the data in Figs. 2–4 show that PEP-19 and PEP(28–62) bind predominately to a single site in the C-domain of CaM. In contrast, there are at least two binding sites for PEP(39–62) on CaM, located in the N- and C-domains.

Comparative Effects of PEP-19 Peptides on Equilibrium Ca^{2+} Binding

Fig. 5*A* and Table 2 compare the macroscopic Ca^{2+} dissociation constants, K_{d1} through K_{d4}, for CaM in the absence or presence of PEP-19 derivatives. Linse *et al.* (21) assigned K_{d1}/K_{d2} and K_{d3}/K_{d4} to Ca^{2+} binding sites in the C- and N-domains of free CaM, respectively. We have adopted these assignments because the binding constants in Table 2 for free CaM are in agreement with those reported by other groups using the same technique under similar conditions (21, 22). Similar to previous reports using a variety of techniques (21, 27–29), Table 2 demonstrates strong positive cooperativity of Ca^{2+} binding to the C-domain of CaM

because $K_{d2} < K_{d1}/4$, with a lower limit for the free energy of cooperativity ($\Delta\Delta G_c$) of −3.4 kcal/mol.

Table 2 shows that intact PEP-19 and PEP(28–62) have little effect on K_{d3} or K_{d4}, but have significant effects on K_{d1} and K_{d2}. Because both PEP-19 and PEP(28–62) have relatively small effects on amide chemical shifts in the N-domain (see Fig. 2), we have assigned K_{d3} and K_{d4} as macroscopic binding constants for the N-domain, and K_{d1} to K_{d2} to the C-domain of CaM bound to either PEP-19 or PEP(28–62). Both PEP-19 and PEP(28–62) cause a significant decrease in the cooperativity of Ca^{2+} binding to the C-domain of CaM from a $\Delta\Delta G_c$ of −3.4 to −1.3 kcal/mol. PEP(39–62) has little effect on K_{d2}, K_{d3}, or K_{d4}, but increases the affinity of binding the first Ca^{2+} (K_{d1}) from 17 μM with free CaM to 1.4 μM in the presence of the peptide. This results in a lower degree of cooperativity of Ca^{2+} binding to the putative C-domain of CaM, but a 3-fold increase in overall affinity.

Comparative Effects of PEP-19 Peptides on Ca^{2+} Binding Kinetics

The rate of dissociation of Ca^{2+} from the N-domain of CaM is very fast and occurs within the dead-time of the stopped-flow fluorimeter at room temperature (1.7 ms). Thus, only the slower release of two Ca^{2+} ions from the C-domain of CaM can be readily detected. Fig. 5*B* and Table 3 show that both intact PEP-19 and PEP(28–62) greatly increase the rate of dissociation of Ca^{2+} from CaM. PEP-19 has a similar effect on a recombinant CaM C-terminal fragment, CaM-(76–148), which further supports its domain-specific effect, and assignment of K_{d1} and K_{d2} in Table 2 to the C-domain of CaM. In contrast, the shorter PEP(39–62) has the opposite effect of decreasing the observed rate of Ca^{2+} dissociation by about 3-fold. The magnitude of this slow phase is consistent with the release of 2 Ca^{2+} ions from the C-domain, and the 3-fold decrease in rate would account for the higher affinity of Ca^{2+} binding to the C-domain in the presence of PEP(36–62) shown in Table 2.

"Experimental Procedures" describes an assay to measure Ca^{2+} k_{on} rates at free Ca^{2+} levels maintained between 0.5 and 5 μM using Br_2BAPTA as both a Ca^{2+} buffer and a chromophore to monitor Ca^{2+} binding to CaM. EGTA was used in control experiments, because its high affinity for Ca^{2+} at pH 7.5 (K_d = 0.038 μM) ensures saturation at all levels of free Ca^{2+} used in the assay, but the Ca^{2+} association rate for EGTA is easily measured using stopped-flow techniques. Fig. 5*C* shows the expected increase in rate of association of Ca^{2+} with EGTA at increasing free Ca^{2+} levels.

Fig. 5*D* shows the rate of Ca^{2+} binding to CaM at free Ca^{2+} levels ranging from about 0.5 to 5 μM. The data best fit a single exponential rate at all Ca^{2+} levels. The increased magnitude of change at higher free Ca^{2+} levels is consistent with an increased percent saturation of the C-domain with Ca^{2+}, which has an overall K_d of 2.3 μM. We observed no effect of either PEP(39–62) or PEP(29–45) on the rate of Ca^{2+} binding to CaM, however, Fig. 5*E* shows that both intact PEP-19 and PEP(28–62) greatly increased the observed Ca^{2+} k_{on}.

DISCUSSION

The primary goal of the current study was to define residues in PEP-19 that modulate Ca^{2+} binding to CaM. During the course of these experiments we also showed that PEP-19 attenuates the degree of positive cooperativity of Ca^{2+} binding to sites III and IV. Positive cooperativity simply means that binding the first Ca^{2+} ion increases the affinity of binding the second Ca^{2+}. With respect to the macroscopic binding constants K_{d1} and K_{d2} shown in Fig. 6*A*, positive cooperativity is implied if $K_{d2} < K_{d1}/4$. Because $K_d = k_{off}/k_{on}$, this criteria can be satisfied by a wide range of rate constants. It is therefore not immediately apparent from macroscopic Ca^{2+} binding constants how changes in cooperativity could account for the large effects of PEP-19 on the rates of Ca^{2+} binding.

Little is known about the microscopic equilibrium Ca^{2+} binding and rate constants for CaM, but it is these parameters that would provide the greatest insight into the mechanism of action of PEP-19. Thus, we developed a kinetic model for cooperative Ca^{2+} binding to CaM that is based on experimental data and algebraic expressions that relate microscopic and macroscopic binding and rate constants (see "Experimental Procedures" for details). The model was used to derive and optimize the microscopic rate constants shown in Fig. 6*A* for transition of the C-domain of CaM from the 0-Ca^{2+} to 2-Ca^{2+} states. The models were tested by comparing experimental data with a simulation using rate constants derived from the model to predict the pseudo first-order rate of association of Ca^{2+} with the C-domain of CaM. Fig. 6*B* shows that the simulation closely approximates the experimental data, with both data sets showing a non-linear relationship between free Ca^{2+} and the rate of Ca^{2+} binding.

A key feature of the kinetic model described in Fig. 6 is that binding the first Ca^{2+} ion to either site III or IV is characterized by fast rate constants, whereas binding the second Ca^{2+} occurs with much slower rates. In essence, binding the first Ca^{2+} to either site III or IV increases the affinity of binding the second Ca^{2+}, which defines positive cooperativity, but it also drastically slows the rates of this second binding event. This immediately implies that the observed attenuation of cooperativity by PEP-19 could accelerate Ca^{2+} rate constants by allowing greater expression of rapid rates associated with independent binding of Ca^{2+} to sites III and IV.

Our results demonstrate that the core IQ sequence (amino acids 39–62) is necessary to promote binding of PEP-19 to CaM, but that it does not mimic other properties of PEP-19. The core IQ motif binds to at least two sites on CaM. One site has a K_d similar to that of binding intact PEP-19, whereas another site binds the IQ motif with higher affinity. This must be considered when evaluating data that utilize IQ peptides taken out of context of the intact protein. For example, our results are consistent with a previous report showing that a synthetic peptide called camstatin, which spans the IQ motif in PEP-19 (residues 36–60), was a more effective inhibitor of nNOS than intact PEP-19 (36). It is likely that the properties of camstatin are similar to those of PEP(39–62). Although intact PEP-19 binds to Ca^{2+}-CaM with relatively low affinity (K_d of 20 to 30 μM), it is present at high concentrations in brain (39), and the *inset* to Fig. 5 shows that PEP-19 at a concentration of 5 μM significantly increases the rate of dissociation of Ca^{2+} from CaM.

Our data show that coupling the acidic-rich amino acids 28–40 to the core IQ motif is necessary to mimic intact PEP-19 with respect to preferential binding to the C-domain of CaM, and modulating Ca^{2+} binding to sites III and IV. This defines the functionally relevant region of PEP-19 to a short acidic/IQ motif of 35 amino acids. The presence of this motif in other proteins (see Fig. 1) implies a functional significance that extends beyond PEP-19. Of particular interest are large proteins that may have intrinsic activity, such as the sea urchin protein in Fig. 1*A* that also encodes fibronectin type II and multiple PLAT/LH2 domains. The acidic/IQ motif may mediate direct CaM-dependent regulation of larger proteins, with modulation of Ca^{2+} binding to CaM as an integral feature of this regulation.

A critical role for acidic residues in modulating Ca^{2+} binding to CaM implies mechanisms involving interactions between Ca^{2+} and PEP-19. The acidic region may function as a negatively charged antenna that electrostatically "steers" Ca^{2+} ions to and from sites III and IV. A more specific interaction with Ca^{2+} is suggested by the primary sequence in Fig. 1*A*. With the exception of Pro-37, residues Glu-29 to Glu-40 in PEP-19 conform well to the consensus sequence of an EF-hand Ca^{2+} binding loop, with oxygen-containing side chains at coordination positions X, Y, Z, −Y, and −Z. Interestingly, the acidic region of RC3 does not

have a similar distribution of acidic residues. The role of this putative Ca^{2+} binding loop is currently being studied.

Synergy between the core IQ sequence and adjacent residues to achieve unique functionality is a paradigm that may apply to other IQ motif proteins. For example, residues N-terminal to the IQ motif of $Ca_V1.2$ are not highly acidic. Instead, this sequence includes a Phe residue (see *open arrow* in Fig. 1*A*) that anchors $Ca_V1.2$ to the N-domain of CaM (see *open arrow* in Fig. 1*A*) (11, 12). This region of $Ca_V1.2$ may play an important regulatory role because channel facilitation and inactivation is thought to be mediated by dynamic differential binding of the N- and C-domains of CaM to the IQ region (15). A corresponding Phe residue is not present in PEP-19. Thus, different modules extending N-terminal to the IQ motifs of PEP-19 *versus* $Ca_V1.2$ appear to confer unique functionalities to these CaM binding proteins.

In summary, this study reports a comprehensive new kinetic model that can account for cooperative Ca^{2+} binding to the C-domain of CaM and provides a mechanistic model for the effects of PEP-19 at the level of attenuating cooperativity. We also show that the effects of PEP-19 on CaM rely on the synergy between the core IQ motif that targets PEP-19 to CaM, and an adjacent acidic cluster that modulates Ca^{2+} binding. We propose that this acidic/IQ motif is a regulator of CaM signaling found in diverse proteins and species.

References

1. Chin D, Means AR. Cell Biol. 2000; 10:322–328.
2. Berridge MJ, Bootman MD, Roderick HL. Nat Rev. 2003; 4:517–525.
3. Bootman M, Lipp P, Berridge MJ. J Cell Sci. 2002; 114:2213–2222. [PubMed: 11493661]
4. Rakhilin SV, Olson PA, Nishi A, Starkove NN, Fienberg AA, Nairn AC, Surmeier DJ, Greengard P. Science. 2004; 306:698–701. [PubMed: 15499021]
5. Putkey JA, Kleerekoper Q, Gaertner TR, Waxham MN. J Biol Chem. 2003; 278:49667–49670. [PubMed: 14551202]
6. Gaertner TR, Putkey JA, Waxham MN. J Biol Chem. 2004; 279:9374–9382.
7. Pak JH, Huang FL, Li J, Balschun D, Reymann KG, Chiang C, Westphal H, Huang KP. Proc Natl Acad Sci U S A. 2000; 97:11232–11237. [PubMed: 11016969]
8. Wu J, Li J, Huang KP, Huang FL. J Biol Chem. 2002; 277:19498–19505. [PubMed: 11912190]
9. van Dalen JJ, Gerendasy DD, de Graan PN, Schrama LH, Gruol DL. Eur J Neurosci. 2003; 18:13–22. [PubMed: 12859333]
10. Rhoads A, Bahler M. FEBS Lett. 2002; 513:107–113. [PubMed: 11911888]
11. Fallon JL, Halling DB, Hamilton SL, Quiocho FA. Structure. 2005; 13:1881–1886. [PubMed: 16338416]
12. Van Petegem F, Chatelain FC, Minor DL Jr. Nat Struct Mol Biol. 2005; 12:1108–1115. [PubMed: 16299511]
13. Cui Y, Wen J, Hung Sze K, Man D, Lin D, Liu M, Zhu G. Anal Biochem. 2003; 315:175–182. [PubMed: 12689827]
14. Trybus KM, Gushchin MI, Lui H, Hazelwood L, Krementsova EB, Volkmann N, Hanein D. J Biol Chem. 2007; 282:23316–23325. [PubMed: 17562702]
15. Liang H, DeMaria CD, Erickson MG, Mori MX, Alseikhan BA, Yue DT. Neuron. 2003; 39:951–960. [PubMed: 12971895]
16. Xiong L, Kleerekoper QK, He R, Putkey JA, Hamilton SL. J Biol Chem. 2005; 280:7070–7079. [PubMed: 15583004]
17. Putkey JA, Donnelly PV, Means AR. Methods Enzymol. 1987; 139:303–317. [PubMed: 3473274]
18. Putkey JA, Waxham MN. J Biol Chem. 1996; 271:29619–29623. [PubMed: 8939892]
19. Peng JW, Wagner G. Biochemistry. 2004; 34:16733–16752. [PubMed: 8527448]

20. Waxham MN, Tsai AL, Putkey JA. J Biol Chem. 1998; 273:17579–17584. [PubMed: 9651352]
21. Linse S, Helmersson A, Forsén S. J Biol Chem. 1991; 266:8050–8054. [PubMed: 1902469]
22. Bayley PM, Findlay WA, Martin SR. Protein Sci. 1996; 5:1215–1228. [PubMed: 8819155]
23. Maune JF, Klee CB, Beckingham K. J Biol Chem. 1992; 267:5286–5295. [PubMed: 1544911]
24. Johnson JD, Snyder C, Walsh C, Flynn M. J Biol Chem. 1996; 271:761–767. [PubMed: 8557684]
25. Peersen OB, Madsen TS, Falke JJ. Protein Sci. 1997; 6:794–807. [PubMed: 9098889]
26. Pedigo S, Shea MA. Biochemistry. 1995; 34:10676–10689. [PubMed: 7654722]
27. VanScyoc WS, Sorensen BR, Rusinova E, Laws WR, Ross JA, Shea MA. Biophys J. 2002; 83:2767–2780. [PubMed: 12414709]
28. Sorensen BR, Shea MA. Biochemistry. 1998; 37:4244–4253. [PubMed: 9521747]
29. Biekofsky RR, Matin SR, Browne JP, Bayley PM, Feeney J. Biochemistry. 1998; 37:7617–7629. [PubMed: 9585577]
30. Ulmer TS, Soelaiman S, Li S, Klee CB, Tang WJ, Bax A. J Biol Chem. 2003; 278:29261–29266. [PubMed: 12724328]
31. Haiech, J.; Kilhoffer, M-C. Calcium-binding Protein Protocols. 173. Vol. II. Humana Press; Totowa, NJ: 2002. p. 25-42.
32. Evanas J, Thulin E, Malmendal A, Forsen S, Carlstrom G. Biochemistry. 1997; 36:3448–3457. [PubMed: 9131994]
33. Evenas J, Malmendal A, Akke M. Structure. 2001; 9:185–195. [PubMed: 11286885]
34. Martin SR, Maune JF, Beckingham K, Bayley PM. Eur J Biochem. 1992; 205:1107–1114. [PubMed: 1576994]
35. Persechini A, White HD, Gansz KJ. J Biol Chem. 1996; 271:62–67. [PubMed: 8550626]
36. Slemmon JR, Morgan JI, Fullerton SM, Danho W, Hilbush BS, Wengenack TM. J Biol Chem. 1996; 271:15911–15917. [PubMed: 8663125]
37. Torok K, Tzortzopoulos A, Grabarek Z, Best SL, Thorogate R. Biochemistry. 2001; 40:14878–14890. [PubMed: 11732908]
38. Meador WE, Means AR, Quiocho FA. Science. 1993; 262:1718–1721. [PubMed: 8259515]
39. Slemmon JR, Feng B, Erhardt JA. Mol Neurobiol. 2001; 22:99–113. [PubMed: 11414283]

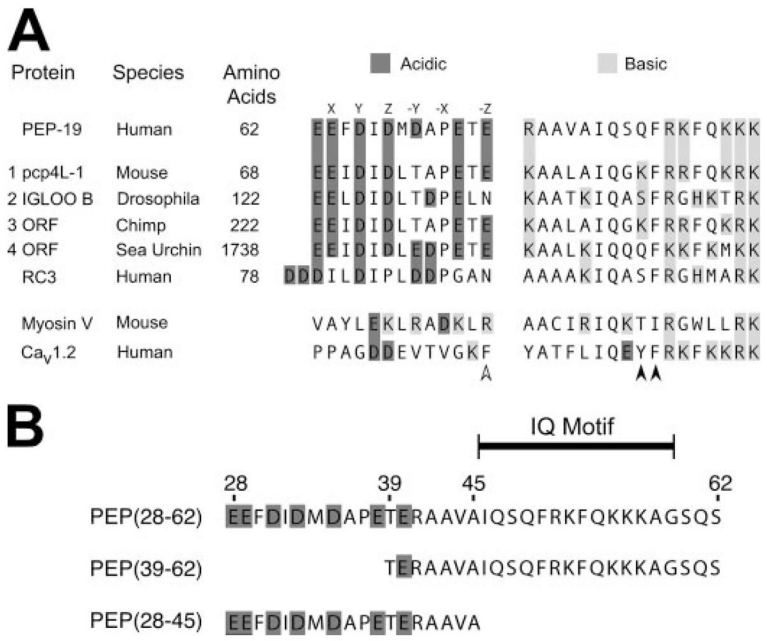

FIGURE 1. Sequence alignment of PEP-19 with residues in other proteins

A protein BLAST similarity search was performed using the NCBI web server to compare PEP-19 residues 25–62 with all non-redundant sequences in GenBank CDS translations, RefSeq proteins, PDB, SwissProt, PIR, and PRF databases. *Panel A* shows the sequence similarity between PEP-19 and 4 of 149 BLAST hits. Also shown are the corresponding regions from RC3, myosin V, and voltage-gated Ca^{2+} channel ($Ca_V1.2$). The *letters above* residues in the PEP-19 sequence are the relative positions of amino acids that coordinate Ca^{2+} in a consensus EF-hand (see text for details). The accession numbers for BLAST hits 1 to 4 are: AY304481.1, NP_477061, XM_001152960.1, and XM_787004.2. *Panel B* shows sequences for PEP-19 synthetic peptides used in the current study. The indicated IQ motif is based on a comparison of numerous IQ motif proteins (10), and the minimal region in PEP-19 that has CaM antagonist activity (36).

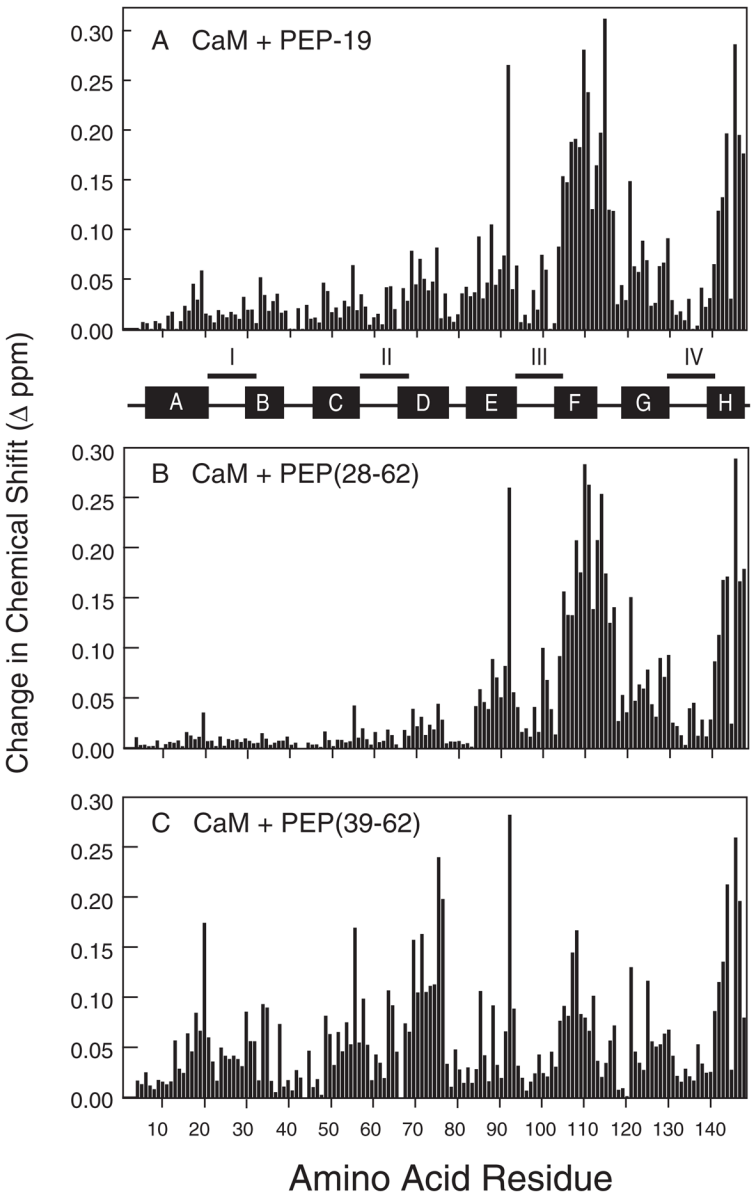

FIGURE 2. Comparative effects of PEP-19 (*panel A*), PEP(28–62) (*panel B*), and PEP(39–62) (*panel C*) on the amide chemical shifts of Ca^{2+}-CaM

Chemical shift changes were calculated as described under “Experimental Procedures.”

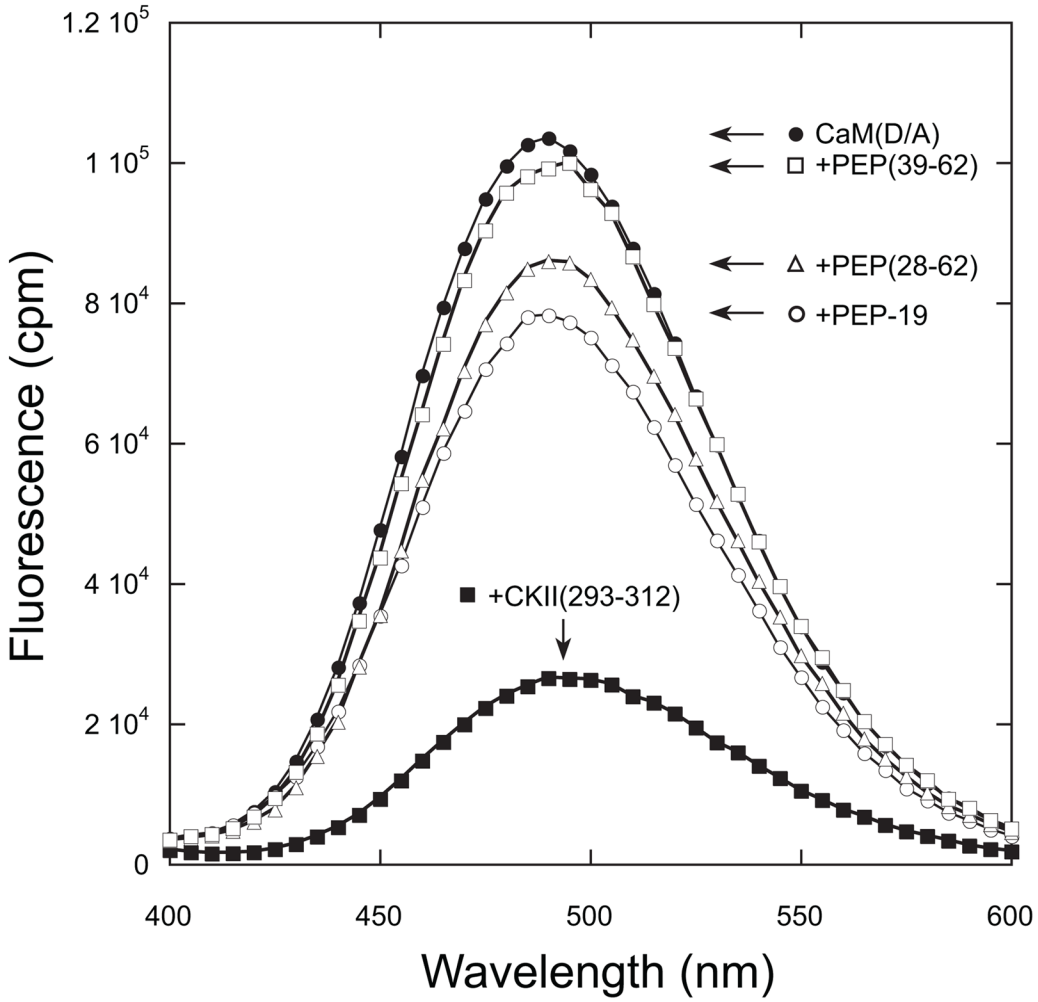

FIGURE 3. Effect of PEP-19 polypeptides on the global conformation of CaM

The fluorescence emission spectrum of CaMD/A was compared in the absence or presence of PEP-19, PEP(28–62), PEP(39–62), or CKII-(293–312). Spectra were collected in solutions of 10 mM MOPS, pH 7.5, 100 mM KCl, 0.1 mM $CaCl_2$, and 1 μM CaMD/A. All PEP-19 derivatives were present at 60 μM, whereas CKII-(293–312) was present at 4 μM. The excitation wavelength was 335 nm, and spectra were corrected for the effect of the various polypeptides on fluorescence from CaM labeled with the FRET donor alone as described under “Experimental Procedures.”

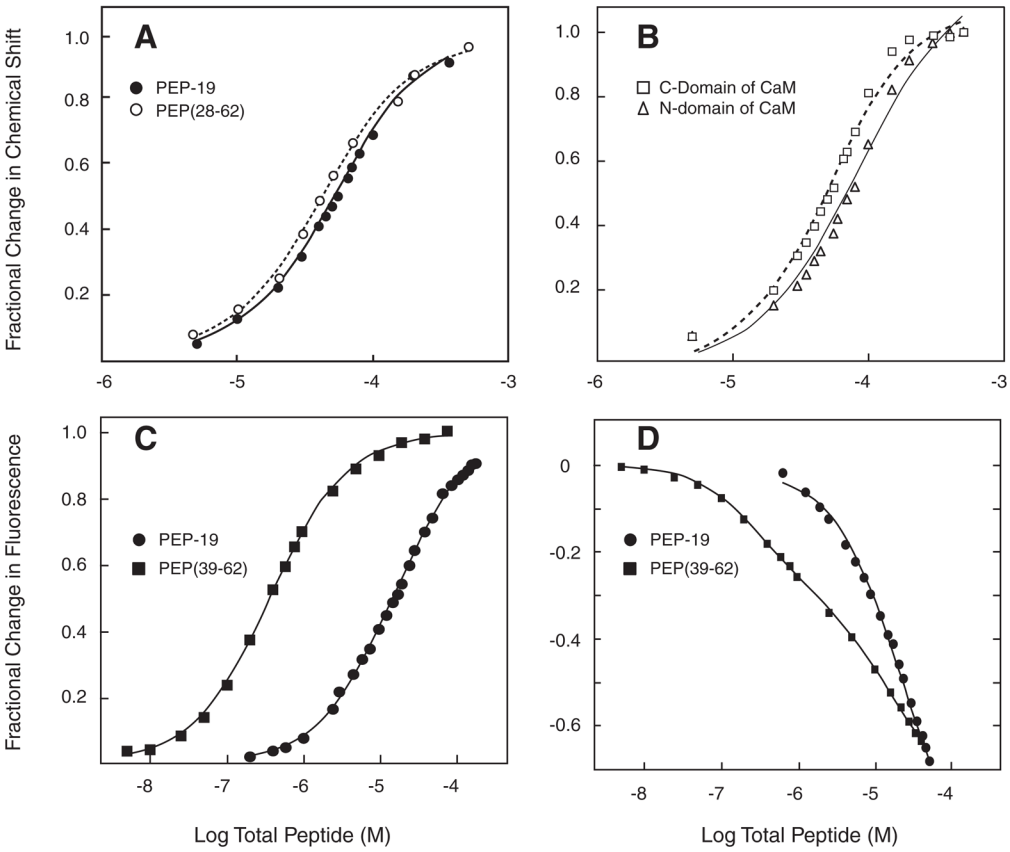

FIGURE 4. Equilibrium binding of PEP-19 polypeptides to CaM

Panel A shows the fractional change in amide chemical shifts in the C-domain of Ca^{2+}-CaM as a function of increasing concentrations of either PEP-19 (*closed circles*) or PEP(28–62) (*open circles*). The data represent the average fractional change for ^{1}H and or ^{15}N nuclei for residues 99, 105, 109, 116, 121, 146, and 147. The *line* represents the fit to a single-site binding model described under "Experimental Procedures." *Panel B* shows the average fractional change in chemical shifts for residues 5, 17, 19, 21 29, 33, 44, 53, 55, 57, 64, 70, and 73 in the N-domain (*open squares*) and residues 94, 105, 106, 110, 116, 117, 130, 137, 146, 147, and 148 in the C-domain (*open triangles*) of Ca^{2+}-CaM as a function of increasing concentrations of PEP(39–62). Chemical shift changes in response to PEP(39–62) did not fit well to a single-site binding model. *Panel C* shows the change in fluorescence from CaM_{ACR} upon titration with PEP-19 or PEP(39–62). *Panel D* shows titration of IAEDANS-labeled CaM(T110C) with DDPM-labeled PEP-19 or PEP(39–62). Labeled CaM for experiments in both *panels C* and *D* was present at 0.05 or 0.5 μM for titration with PEP(39–62) or PEP-19, respectively.

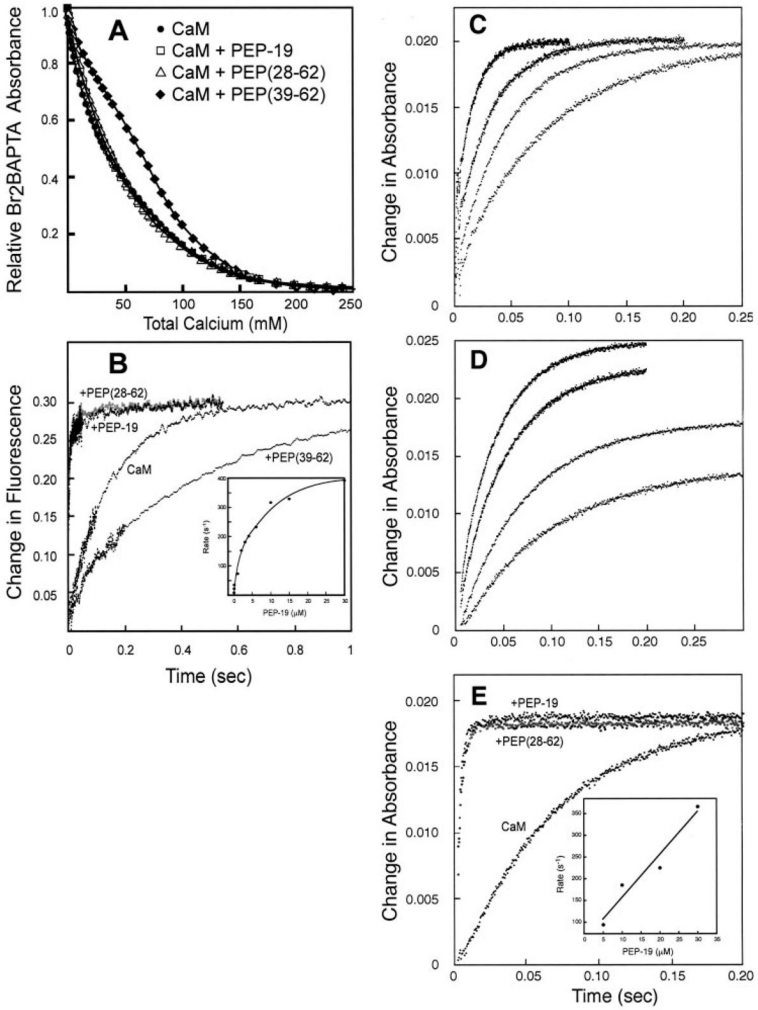

FIGURE 5. Effects of PEP-19 polypeptides on Ca^{2+} binding to CaM

Panel A shows equilibrium Ca^{2+} binding to CaM in the presence of PEP-19, PEP(28–62), or PEP(39–62). The *lines* show a least-squares fit of the data to the algorithm described under "Experimental Procedures." *Panel B* shows the rate of dissociation of Ca^{2+} from free CaM (2 μM), and in the presence of 30 μM PEP-19, PEP(28–62) (*gray circles*), or PEP(39–62). The *inset* to *panel B* shows the effect of increasing concentrations of PEP-19 on the rate of dissociation of Ca^{2+} from the C-domain of CaM (2 μM). A single rate was observed at concentrations of PEP-19 > 2 μM, whereas Ca^{2+} dissociation at concentrations of PEP-19 of <2 μM best fit an exponential decay with two rate constants. For these data points, a weighted average rate was determined from $(R_1 \times A_1 + R_2 \times A_2)/(A_1 + A_2)$. *Panel C* shows the rate of change in absorbance when a solution of EGTA (2 μM) was rapidly mixed with Br_2BAPTA solutions of increasing free Ca^{2+} levels as described under "Experimental Procedures." All data sets best fit a single exponential equation. The observed rate was used to calculate the free Ca^{2+} levels in the optical chamber (see "Experimental Procedures") for the various Ca^{2+} /BrBATPA buffer solutions as 0.9, 1.6, 2.3, and 4.8 μM. *Panel D* shows the rate of change in absorbance when a solution of apo-CaM (2 μM) was rapidly mixed with Br_2BAPTA solutions with free Ca^{2+} levels of 0.9, 1.6, 2.3, and 2.9 μM Ca^{2+} levels used in the experiments in *panel C*. All data sets best fit a single exponential equation. *Panel E* compares the rate of change in absorbance when a Ca^{2+} /Br_2BAPTA solution with a free

Ca^{2+} level of 3μM was rapidly mixed with apo-CaM with or without 30 μM PEP-19 or PEP(28–62) (*gray circles*).

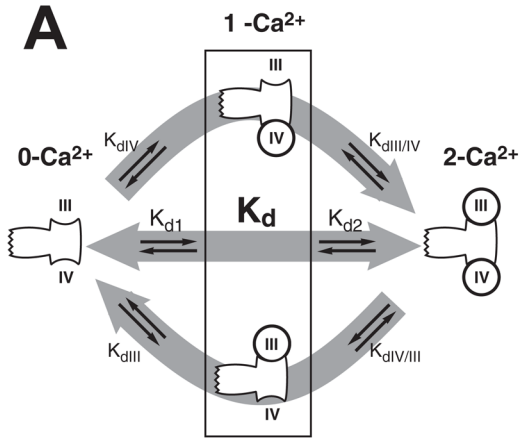

	Binding Event	K_d (μM)	k_{on} ($\mu M^{-1}s^{-1}$)	k_{off} (s^{-1})
First Ca^{2+}	IV	18.5	275	5.1×10^3
	III	117	275	32×10^3
Second Ca^{2+}	IV/III	0.05	**40.1**	**1.9**
	III/IV	0.30	**29.9**	**9.0**

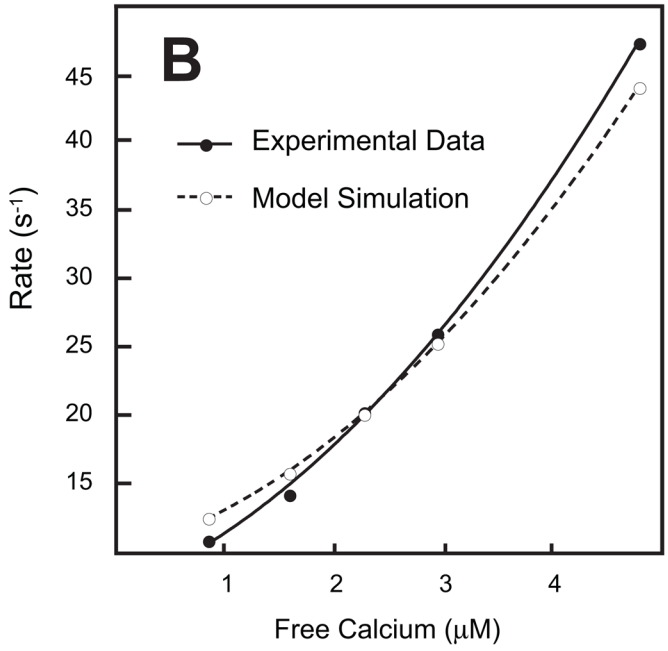

FIGURE 6. Cooperative Ca^{2+} binding to the C-domain of CaM

Panel A illustrates the microscopic equilibrium Ca^{2+} binding reactions associated with transition of the C-domain of CaM from the 0-Ca^{2+} to 2-Ca^{2+} states. The table in *panel A* lists optimized equilibrium and kinetic microscopic Ca^{2+} binding constants derived as described under "Experimental Procedures." *Panel B* shows the relationship between observed Ca^{2+} association rates at free Ca^{2+} in the range of 1 to 5 μM. The *closed circles* are experimental data derived as described in the legend to Fig. 5*E* and under "Experimental Procedures." The *open circles* are derived from a simulation carried out using the model described under "Experimental Procedures" and the binding parameters shown in *panel A*.

TABLE 1

Dissociation constants (μM) for Binding CaM to PEP-19, PEP(28–62), and PEP(39–62)

Assay	PEP-19	PEP(28–62)	PEP(39–62)	
			K_{d1}	K_{d2}
NMR[a]	29 ± 0.7	24 ± 0.8	—[b]	—
Fluorescence[c]	18 ± 3	ND[d]	0.24 ± 0.04	—
FRET	20 ± 4	ND	0.16 ± 0.05	27 ± 3

[a]Values are the average mean ± S.E. of K_d values derived separately from chemical shift changes for ^{1}H and/or ^{15}N nuclei of amides for residues 99, 105, 109, 116, 117, 146, and 147.

[b]NMR data fit poorly to either single or two-site binding models. Fluorescence data fit best to a single-site binding model.

[c]The values derived from fluorescence and FRET data are the mean ± S.E. of three to four experiments.

[d]ND, not determined.

TABLE 2

Effect of PEP-19, PEP(28–62), and PEP(39–62) on calcium binding affinity and cooperativity

The macroscopic dissociation constants were derived as described in Material and Methods. All values are the average mean ± S.E. of (n) independent titrations. The square root of the product of macroscopic dissociation constants for each domain is equivalent to the K_{Ca50} for binding to each domain. The precision of this value is greater than the individual dissociation constants. The overall decrease in free energy from binding two Ca^{2+} ions to the N- or C-domains (ΔG_{tot}) was calculated as $\Delta G_{tot} = -RT\ln(K_1 \times K_2)$. The upper limit for the change in free energy due to cooperative Ca^{2+} binding ($\Delta\Delta G_c$) was calculated as $\Delta\Delta G_c = -RT\ln(4 \times K_2/K_1)$. Free energy values are in kcal/mole.

		C-Domain					N-Domain				
		Macroscopic K_d (μM)					Macroscopic K_d (μM)				
	N	K_{d1}	K_{d2}	$\sqrt{K_{d1}{}^{*}K_{d2}}$	ΔG_{tot}	$\Delta\Delta G_c$	K_{d3}	K_{d4}	$\sqrt{K_{d3}{}^{*}K_{d4}}$	ΔG_{tot}	$\Delta\Delta G_c$
CaM	(15)	17 ± 3	0.4 ± 0.1	2.2 ± 0.2	−15.3 ± 0.3	−3.4 ± 0.3	34 ± 4	6.2 ± 1	13.1 ± 1.0	−13.3 ± 0.1	−1.9 ± 0.2
CaM + PEP-19	(6)	4.7 ± 1	2.0 ± 0.2	2.8 ± 0.2	−15.0 ± 0.1	−1.3 ± 0.2	35 ± 6	3.9 ± 0.6	14.0 ± 1.0	−13.2 ± 0.1	−2.3 ± 0.2
CaM + PEP(28–62)	(3)	5.0 ± 1.3	1.7 ± 0.3	2.8 ± 0.1	−15.0 ± 0.1	−1.4 ± 0.3	57 ± 25	4.1 ± 1.4	13.1 ± 0.5	−13.2 ± 0.1	−2.3 ± 0.5
CaM + PEP(39–62)	(3)	1.4 ± 0.3	0.4 ± 0.1	0.7 ± 0.1	−16.6 ± 0.1	−1.6 ± 0.3	36 ± 1	2.6 ± 1.0	8.6 ± 0.7	−13.7 ± 0.1	−2.4 ± 0.4

TABLE 3

Effect of PEP-19, PEP(28–62), and PEP(39–62) on Ca^{2+} dissociation from CaM

Condition	k_{off} rate
	(s^{-1})
CaM	9.9 ± 0.4
CaM-(76–148)	12.1 ± 0.2
CaM + PEP-19	430 ± 50
CaM-(76–148) + PEP-19	490 ± 20
CaM + PEP(28–62)	390 ± 40
CaM + PEP(39–62)	3.2 ± 0.3

Dissociation rates (k_{off}) were derived by fitting data such as that in Fig. 5*B* to a single exponential equation. The values are the mean ± S.D. of three to six experiments. CaM was present at 2 to 5 μM, and PEP-19 or PEP-19 peptides were present at 30 μM.